Seismic, anisotropy

Encyclopedia of Solid Earth Geophysics
Harsh Gupta (Ed.)
Springer

Thorsten W. Becker
Associate Professor of Earth Sciences
Department of Earth Sciences
University of Southern California
Los Angeles CA 90089-0740
E-mail: thorstinski@gmail.com
Tel: 1-213-740-8365
Fax: 1-213-740-8801

Becker, T. W. (2010): Seismic Anisotropy, In: Encyclopedia of Solid Earth Geophysics, Gupta, H. (ed.), Springer.

Definition

Seismic anisotropy refers to the directional dependence of seismic wave speeds and particle motion polarizations, as well as the splitting of normal modes, as caused by the elastic properties of rocks.

Introduction

Many of the minerals that make up Earth are intrinsically anisotropic. When rocks are progressively deformed over geologic timescales, the alignment of mineral grains (lattice preferred orientation, LPO) can lead to bulk anisotropy of the rock. Bulk anisotropy can additionally be generated by an ordered assembly of individually isotropic materials of different wave speeds (shape preferred orientation, SPO). Both types of anisotropy are found within the Earth; SPO anisotropy also highlights a fundamental ambiguity between isotropic heterogeneity and anisotropy. Seismic wave propagation through an anisotropic medium depends on the wavelengths over which a particular wave type averages, complicating the analysis of seismological data. Both LPO and SPO imply significantly different (up to $\sim$10%) speeds for waves of different polarization or propagation directions, and velocity variations can be larger than those expected from compositional or thermal heterogeneity. Seismic anisotropy is therefore of fundamental importance for structural imaging studies. To get robust estimates of the quantities of interest for geodynamic interpretation, the trade-off between isotropic and anisotropic structure has to be considered. Seismic anisotropy provides a powerful link between seismic observations and the dynamic processes that shape the solid Earth, for example convective flow in the case of LPO in the mantle (Figure 1, see *Mantle convection*). However, anisotropic tomographic inversions are inherently more non-unique than isotropic imaging (see *Inverse theory*) because a general anisotropic, linearly-elastic medium has 21 independent components of the elasticity tensor, as opposed to two in the isotropic case. As a consequence of the increased number of parameters and the differences in how data sampling constrains isotropic and anisotropic structure, more data are needed for the same level of resolution in an anisotropic inversion. Typically, additional *a priori* constraints, such as from petrology, are needed to narrow the parameter space. These complexities make the study of anisotropy in a geodynamic context inherently multi-disciplinary, involving seismology, mineral physics, rock mechanics, and geodynamic modeling.

Basic mathematical description

Seismic anisotropy arises when the linear elasticity tensor C that connects stress, σ, and strain, ε, tensors as

$$\sigma_{ij} = \sum_{k=1}^{3}\sum_{l=1}^{3} C_{ijkl}\varepsilon_{kl} \qquad (1)$$

Becker, T. W. (2010): Seismic Anisotropy, In: Encyclopedia of Solid Earth Geophysics, Gupta, H. (ed.), Springer.

does not simplify to the isotropic form

$$C_{ijkl} = \lambda\delta_{ij}\delta_{kl} + \mu\left(\delta_{ik}\delta_{jl} + \delta_{il}\delta_{jk}\right), \tag{2}$$

where λ and μ are the first and second (shear modulus) Lamé parameters, δ the Kronecker delta ($\delta_{ij} = 1$ for $i = j$, and 0 else), and the indices run over the three axes of the coordinate system, x_1, x_2, and x_3. In general, C has 81 components, out of which 21 are independent, and the most complex (triclinic) form of anisotropy requires the specification of all those components (*e.g. Hearmon*, 1961; *Nye*, 1985; *Anderson*, 1989). A typical simplification is to assume hexagonal anisotropy, which should capture most aspects of olivine LPO related anisotropy in the upper mantle (*Montagner and Anderson*, 1989; *Browaeys and Chevrot*, 2004; *Becker et al.*, 2006).

If C is expressed in the 6×6 Voigt matrix, c, notation where c_{mn} relates to C_{ijkl} as $m = \delta_{ij}i + (1-\delta_{ij})(9-i-j)$ and $n = \delta_{kl}k + (1-\delta_{kl})(9-k-1)$, then the five *Love* (1927) parameters for the transversely isotropic medium that results from hexagonal symmetry correspond to

$$A = c_{11} = \rho v_{PH}^2, \quad C = c_{33} = \rho v_{PV}^2, \quad L = c_{44} = \rho v_{SV}^2, \quad N = c_{66} = \rho v_{SH}^2, \quad \text{and} \quad F = c_{11}. \tag{3}$$

Here, ρ is density, and $v_{PH,PV}$ the velocities for P waves propagating horizontally (H, in x_1-x_2 plane) and vertically (V, x_3-axis), respectively. For shear waves, $v_{SH,SV}$ in eq. (3) are the velocities for horizontally propagating waves that are horizontally or vertically polarized, respectively (see *Elasticity and wave propagation*). Transverse isotropy as a simplified description of material anisotropy is widely used and developed in exploration seismics (*e.g. Thomsen*, 1986). The top 220 km in the PREM 1D Earth model (*Dziewoński and Anderson*, 1981) are also transversely isotropic with vertical symmetry axis as in eq. (3); such a medium is said to have bulk radial anisotropy. (Note that vertically propagating S waves in this case have the same velocity, v_{SV}, regardless of polarization direction.)

Different combinations of the Love parameters or c_{nm} are used in the literature (*e.g. Babuška and Cara*, 1991); for example, anisotropy in PREM is described by two measures of shear and compressional wave anisotropy strength,

$$\xi = \left(\frac{v_{SH}}{v_{SV}}\right)^2 = \frac{N}{L} \quad \text{and} \quad \phi = \left(\frac{v_{PV}}{v_{PH}}\right)^2 = \frac{C}{A}, \tag{4}$$

respectively, and the parameter $\eta = F/(A-2L)$, which controls how velocities change between the vertical and horizontal direction. Another way to characterize the anisotropy of a transversely isotropic medium is due to *Thomsen* (1986), who defined

$$\varepsilon = \frac{c_{11}-c_{33}}{2c_{33}} = \frac{A-C}{C} \quad \text{and} \quad \gamma = \frac{c_{66}-c_{44}}{2c_{44}} = \frac{N-L}{L} \tag{5}$$

as two different measures of the P and S wave anisotropy strength, respectively, and a combined parameter

$$\delta^* = \frac{1}{2c_{33}^2}\left[2\left(c_{13}+c_{44}\right)^2 - \left(c_{33}-c_{44}\right)\left(c_{11}+c_{33}-2c_{44}\right)\right], \tag{6}$$

Becker, T. W. (2010): Seismic Anisotropy, In: Encyclopedia of Solid Earth Geophysics, Gupta, H. (ed.), Springer.

which, for weak anisotropy, simplifies to

$$\delta = \frac{(c_{13}+c_{44})^2-(c_{33}-c_{44})^2}{2c_{33}(c_{33}-c_{44})}. \tag{7}$$

The δ parameter is important for near-vertical P wave propagation and identical to ε for "elliptical" anisotropy (*Thomsen*, 1986). *Mainprice* (2007) provides an account of other combinations of c_{mn} in use to characterize a transversely isotropic medium. Those differ, regrettably, quite substantially in different fields of study.

If the symmetry axis of the hexagonal anisotropy is in the horizontal plane, the anisotropy is termed azimuthal. This means that perpendicular fast and slow axes can be defined for horizontally propagating SV waves, where waves will propagate with $v_{SV1} > v_{SV2}$ along the fast and slow orientations, respectively. Any perturbations to phase velocity p, δp, due to general, but small anisotropy can be expressed as a series of isotropic, π-periodic, and $\pi/2$ periodic terms (*e.g. Backus*, 1965; *Forsyth*, 1975):

$$\frac{\delta p}{p} \approx A_0 + A_1\cos(2\Psi) + A_2\sin(2\Psi) + A_3\cos(4\Psi) + A_4\sin(4\Psi). \tag{8}$$

Here, Ψ is the azimuth of wave propagation, and eq. (8) follows from the wave equation and the rank of the elasticity tensor (*Smith and Dahlen*, 1973). For mantle rocks, the 2Ψ terms are expected to be larger than the 4Ψ contributions for Rayleigh waves, which are predominantly sensitive to SV (*Anderson*, 1966; *Montagner and Nataf*, 1986). The 4Ψ terms are expected to be bigger than 2Ψ for Love waves, motivating the focus on Rayleigh waves for azimuthal anisotropy studies (see *Surface waves*).

In general, the wave propagation effects of any elasticity tensor C can be analyzed by considering a plane wave $\mathbf{u} = \mathbf{a}\exp(-i\omega(t-\mathbf{s}\cdot\mathbf{x}))$ with ω angular frequency, and $\mathbf{u}$, $\mathbf{a}$, $\mathbf{s}$, and $\mathbf{x}$ the displacement, polarization, slowness, and location vectors, respectively (see *Elasticity and wave propagation*). $\mathbf{s}$ shall have the normalized direction $\hat{\mathbf{s}}$ and length of $1/p$. Using the momentum equation $\ddot{u}_i = \partial_j \sigma_{ij}$, eq. (1), the definition of the strain tensor, $\varepsilon_{ij} = \frac{1}{2}\left(\partial_i u_j + \partial_j u_i\right)$, C's symmetries, and defining $M_{ij} = \frac{1}{\rho} C_{ijkl}\hat{s}_j\hat{s}_l$, we can write

$$\mathsf{M}\mathbf{a} = p^2\mathbf{a}, \tag{9}$$

which is an eigen problem for the symmetric matrix M. Eq. (9) is called the Christoffel equation (*e.g. Babuška and Cara*, 1991). The eigen vector solutions correspond to one quasi-P and two quasi-S wave directions, and the associated eigenvalues are the density-velocity products ρv_P^2, ρv_{S1}^2, and ρv_{S2}^2. These quantities can be contoured for any elasticity tensor, for example as measured from single crystals, as a function of incidence angle and azimuth, to visualize the anisotropic properties of minerals or rocks in isolation (*e.g. Mainprice*, 2007). To generate more realistic synthetic body waves from three-dimensional (3D) variations in anisotropy, semi-analytical reflectivity methods can be used if anisotropy is assumed to vary only with depth. However, for the general case of 3D variations of anisotropy on scales smaller than a Fresnel zone full, numerical wave propagation solutions are needed.

Becker, T. W. (2010): Seismic Anisotropy, In: Encyclopedia of Solid Earth Geophysics, Gupta, H. (ed.), Springer.

Seismological methods

Seismic anisotropy can be detected in a number of ways which can be broadly classified into body and surface wave methods. The split of a shear wave into a fast and slow polarization direction as discussed for the solutions of eq. (9) is akin to optical birefringence; it is exploited by the most popular method of measuring anisotropy, that utilizing *shear wave splitting* (*Ando et al.*, 1983; *Vinnik et al.*, 1984; *Silver and Chan*, 1991). For lithospheric and mantle applications, one typically considers near-vertical incidence SKS or $SKKS$ core phases (see *Body waves*), because the effects of any source-side anisotropy are removed by the S-to-P-to-S conversion upon traversal of the core. The most common splitting measurement consists of detecting the horizontal orientation of the fast (azimuth Ψ) pseudo-S wave from recorded particle motions, as well as determining the delay time δt between the arrival of the fast and slow S pulses (*e.g. Savage*, 1999; *Long and Silver*, 2009).

Shear wave splitting can be detected using a single earthquake measured at a single station, if wave propagation is out of a symmetry axis, and is a unique indicator for the presence of anisotropy along the ray path. However, only the highly idealized case of a single, transversely isotropic layer with horizontal symmetry axis can be directly interpreted in terms of Ψ and δt. Dipping symmetry axes, non-hexagonal anisotropy, or variations of anisotropy with depth will all cause a dependence of apparent splitting on back-azimuth (*e.g. Schulte-Pelkum and Blackman*, 2003). The non-linear nature of the splitting measurement and layer splitting itself can lead to a bias of sensitivity toward the surface ($\sim$one wavelength under the station), and not simple superposition (*e.g. Saltzer et al.*, 2000). Such complexities make it imperative to strive for good back-azimuthal coverage, requiring the recording of several, suitable earthquakes, which is often a challenge given station-event geometry, or the duration of temporary deployments. If back-azimuth variations are detected, those can be used to make inferences about the variation of anisotropy with depth, which is undefined based on isolated measurements where anisotropy could, in principle, arise anywhere between the core mantle boundary (CMB) and the surface in the case of SKS splitting. If regional S arrivals are used, crossing ray paths can be used to infer 3D variations of anisotropy (*e.g. Abt and Fischer*, 2008). For teleseismic arrivals, the use of sensitivity kernels (*e.g. Chevrot*, 2006; *Long et al.*, 2008) for the multi-channel type of measurement of splitting holds great promise for resolving 3D anisotropy in regions for which close (closer than Fresnel zone width) station spacing is available. Broadly speaking, shear wave splitting is, however, a measurement with good lateral ($\sim$50 km), but fairly poor depth resolution (*Savage*, 1999).

Another single, body-wave arrival method that follows from eq. (9) is to use the orientation of the pseudo-P polarization, which may differ by more than 10° from along-ray, for P polarization anisotropy (*Schulte-Pelkum et al.*, 2001), P_{pol}. A measurement of P_{pol} is sensitive to $\sim$half a wave-length underneath the station. If several, near-horizontal P paths with different azimuths are available, as in the case of the refracted P_n phase, which senses underneath the Moho, velocities can be plotted against azimuth to infer azimuthal anisotropy. This method was used for one of the earliest demonstrations of seismic anisotropy by *Hess* (1964), and a global comparison of P_n and SKS splitting can be found in *Smith and Ekström* (1999). The variations in delay times of teleseismic waves can also be used directly to infer anisotropy in the mantle lithosphere (*e.g. Babuška et al.*, 1984; *Bokelmann*, 2002) by means of a tomographic inversion (see *Earthquake tomography*), but this method requires knowledge of the isotropic variations in wave speeds. This is a challenge for all

Becker, T. W. (2010): Seismic Anisotropy, In: Encyclopedia of Solid Earth Geophysics, Gupta, H. (ed.), Springer.

tomographic approaches to anisotropy because there will always be a trade-off between isotropic and anisotropic heterogeneity in the absence of perfect data coverage (*e.g. Tanimoto and Anderson*, 1985). In terms of their depth-sensitivity, the body wave methods can be ranked, from shallow to deep, as P_n, P_{pol}, SKS, and P delay times (*Schulte-Pelkum and Blackman*, 2003).

At crustal depths, anisotropy can additionally be detected by wide-angle refraction methods (*e.g. Meissner et al.*, 2002, 2006). Orthogonal profiling, for example, may show a mismatch of derived seismic velocities, or a mismatch of refraction and reflection depths that can be interpreted in terms of anisotropic wave propagation. Receiver function methods (*e.g. Park and Levin*, 2002) (see *Seismic, receiver function technique*) yield further evidence of crustal anisotropy from the existence of split pS conversions. Azimuthal variations in radial-transverse receiver function amplitudes are diagnostic of anisotropy *vrs.* tilted structure, and of the amount of anisotropy (*e.g. Savage*, 1998).

A wealth of information about anisotropy arises from the study of *surface waves*. The observation that Love waves, which mainly sense SH, travel faster than Rayleigh waves, which mainly sense SV due to their intrinsic polarities, implies the existence of a mean radial anisotropy in the upper mantle (*Anderson*, 1966; *Dziewoński and Anderson*, 1981). The existence of azimuthal anisotropy was documented for the Pacific by the study of Rayleigh waves (*Forsyth*, 1975), and *Nataf et al.* (1984) presented radially anisotropic, upper-mantle tomography. The current state of tomographic models for global azimuthal and radial anisotropy patterns is discussed by *Montagner* (2007). Surface wave propagation is dispersive, which allows the construction of 3D models of anisotropy (see *Seismic structure of the Earth, global models*). The most easily measured phase-velocity period range for fundamental modes between $\sim$50 and 150 s samples from the lithosphere down to $\sim$300 km depth, and Figure 2a shows azimuthal and radial anisotropy at an asthenopsheric depth of 150 km as well as a global compilation of SKS splitting results. At the shallow end, array methods (*e.g. Deschamps et al.*, 2008) and in particular noise tomography (*e.g. Lin et al.*, 2008) (see *Correlation techniques, ambient noise*) facilitate extending the period range to shorter, crustal periods. Overtones can be used to constrain the deeper mantle, down to the 660 km phase transition (*e.g. Trampert and van Heijst*, 2002; *Lebedev and van der Hilst*, 2008). Lastly, the long-period surface wave equivalent of *free oscillations of the Earth* can provide constraints on the deep Earth, including inner core anisotropy (*e.g. Woodhouse et al.*, 1986; *Tromp*, 2001).

Surface wave studies of anisotropy have fairly good depth sensitivity in that they are able to locate the origin of anisotropic signals in the upper mantle to within $\sim$100 km depth. However, particularly compared to body wave measurements such as SKS splitting, the lateral resolution of surface waves is limited, for isotropic structure to perhaps $\sim$500 km and $\sim$50 km for global and regional models, respectively, at present. Reasons for discrepancies between published tomographic models include the different treatment of crustal corrections and phase velocity measurements, as well as theoretical assumptions about wave propagation. Perhaps more important factors are the globally uneven ray path coverage or regularization choices (see *Inverse theory*).

A complete, 3D model of general seismic anisotropy would allow for more powerful petrological and geodynamic inferences than limited studies which focus only on a few aspects of anisotropy or wave propagation. Given the wide array of seismological observations, a desirable procedure to constrain the full 3D dependence of anisotropy is to compare different measures of anisotropy (*e.g. Montagner et al.*, 2000; *Wüstefeld et al.*, 2009) or to perform a joint inversion (*e.g. Montagner and*

Becker, T. W. (2010): Seismic Anisotropy, In: Encyclopedia of Solid Earth Geophysics, Gupta, H. (ed.), Springer.

Nataf, 1988; *Šíleny and Plomerová*, 1996; *Marone and Romanowicz*, 2007). Sensitivity kernels that account for finite frequency wave propagation effects and the resulting complex 3D structure of a measurement's sensitivity to Earth structure (*e.g. Chevrot*, 2006; *Long et al.*, 2008; *Sieminski et al.*, 2009) can facilitate the relative weighting of different observations. Likewise, the incorporation of petrological constraints (*e.g. Montagner and Anderson*, 1989; *Becker et al.*, 2006) can be used to simplify inversions further (*Panning and Nolet*, 2008; *Chevrot and Monteiller*, 2009).

Origin of anisotropy

The SPO type of anisotropy may be caused by any consistent alignment of entities with different isotropic wave speeds. Examples include lower crustal lamellae structures, cracks, or melt inclusions (*e.g. Mainprice and Nicholas*, 1989; *Weiss et al.*, 1999; *Meissner et al.*, 2006). Crack alignment will be only important for the shallowest crust where it may be indicative of crustal stress (*e.g. Crampin and Chastin*, 2003). Alignment of partial melt pockets may play a role both for shallow, extensional lithospheric domains, such as underneath mid-oceanic spreading centers or intracontinental rifts (*e.g. Holtzman et al.*, 2003), and at the base of the mantle in the *Mantle D" Layer* (*e.g. Moore et al.*, 2004).

In between, the LPO type of anisotropy caused by the alignment of intrinsically anisotropic crystals is the most likely cause of anisotropy. The fundamental symmetry classes of material anisotropy of the constituent minerals (*e.g. Nye*, 1985; *Anderson*, 1989) determine the overall type of anisotropy in the Earth, and wave propagation depends critically on the type of anisotropy (*e.g. Levin and Park*, 1998; *Schulte-Pelkum and Blackman*, 2003). Several crustal rocks show LPO anisotropy; of particular interest are those rich in phyllosilicates (micas) in the upper-middle crust, and amphibole minerals in lower crust (*e.g. Christensen and Mooney*, 1995). In the upper mantle, the highly anisotropic olivine makes up $\sim$60% of rocks (*e.g. Mainprice*, 2007). Laboratory experiments show that if multi-crystal olivine assemblages are deformed in the dislocation creep regime, crystals typically align such that the resulting fast propagation orientation rotates into the direction of shear, and many mantle xenoliths show corresponding LPO patterns (*Mainprice*, 2007; *Karato et al.*, 2008).

This connection between rock deformation and seismic anisotropy allows an association of the patterns of azimuthal mantle anisotropy (*e.g.* Figure 2a) with *mantle convection* (*e.g. McKenzie*, 1979; *Tanimoto and Anderson*, 1984). A coarse approximation uses tectonic plate motion to imply deep flow direction, or, more realistically, flow can be calculated from global circulation models (*Hager and O'Connell*, 1981). The general association between mantle flow and anisotropy in terms of radial anisotropy is that flow in the upper boundary layer aligns olivine such that $v_{SH} > v_{SV}$ underneath oceanic plates due to a simple shear type of deformation (Figure 1). In regions of dominantly radial mass transport such as subduction zones and underneath spreading centers, $v_{SV} > v_{SH}$ (*Chastel et al.*, 1993; *Montagner*, 2007). The radial and azimuthal anisotropy patterns shown in Figure 2a are broadly consistent with this expectation (Figure 2b), though there are also clear differences which are easier to constrain in regional studies (*e.g. Gaherty et al.*, 1996). Complexities include variations azimuthal anisotropy orientations and amplitudes (*e.g. Ekström and Dziewonski*, 1998; *Smith et al.*, 2004), and many of those patterns are accessible to geodynamic modeling, discussed below.

Given the importance of the details of the connection between seismology and geodynamics, several theoretical descriptions exist that predict micro-structural LPO development given general deformation histories, as constrained by laboratory experiments (*e.g. Kaminski and Ribe*, 2001; *Blackman*, 2007). However, further laboratory constraints, for example on the reorientation of existing LPO fabrics under changing deformation regimes, are required to decide on the most appropriate treatment. Complex deformation histories are expected to lead to complex anisotropy. Yet, under monotonous deformation (*e.g.* by simple shear), olivine LPO is expected to saturate over finite strains of $\sim$10. Amplitude variations compared to a single crystal may therefore be mainly due to orientation of the symmetry axis of the effective elastic tensor for an aggregate of crystals (*cf. Karato et al.*, 2008).

Laboratory work over the last ten years has further shown that the role of water content, deviatoric stress levels, and pressure can lead to significantly different LPO development from the typical, dry A-type fabrics that show the “fast axes along flow” alignment discussed above. For example, the high stress, high water content B-type fabric aligns the fast axes of olivine orthogonal to the direction of shear. Variations in water content have been used to explain some of the variability that is apparent in asthenospheric depth anisotropy, such as the decrease in azimuthal anisotropy strength across the Pacific from young to older seafloor, or the variability of orientations of SKS splitting in subduction zones (*Mainprice*, 2007; *Karato et al.*, 2008).

LPO development under deformation of mantle rocks not only affects seismic properties, but also leads to thermal and mechanical anisotropy. The feedback of these effects into mantle convection and lithospheric deformation are potentially profound (*e.g. Christensen*, 1987; *Chastel et al.*, 1993; *Lev and Hager*, 2008; *Tommasi et al.*, 2009) and are currently an active area of research.

Observations of anisotropy and dynamic inferences

Whole Earth anisotropy

Seismic anisotropy is found throughout the Earth, with the exception of the fluid outer core, though it is concentrated in certain depth regions (Figure 1). In the mantle, the best constrained and strongest signal is found in the uppermost $\sim$300 km where SH velocities are faster than SV by up to $\sim$4% on average, as indicated by the Love-Rayleigh discrepancy. The exact shape of the average radial anisotropy profile is less certain, though most recent models agree that the largest anomalies are not found at the surface, but rather at $\sim$100 km depth (Figure 2b). This peak may be associated with asthenospheric shear flow which is expected to lead to the largest strain-rates underneath the oceanic lithosphere, which is up to $\sim$100 km thick when defined thermally (see *Mantle convection*). Given that mantle anisotropy is most likely caused by LPO of olivine, the peak in seismic anisotropy in the uppermost mantle has been associated with the relatively high stress and low temperature depth region where dislocation dominates over diffusion creep (*Karato*, 1992; *Gaherty and Jordan*, 1995) (see *Mantle rheology*). Using composite rheologies, geodynamic models can be used to estimate the transition depths for the different creep laws, so delineating the region where LPO forms explicitly (*e.g. McNamara et al.*, 2002; *Podolefsky et al.*, 2004; *Becker et al.*, 2008). Once rocks transition into the diffusion-creep dominated deformation regime, LPO

Becker, T. W. (2010): Seismic Anisotropy, In: Encyclopedia of Solid Earth Geophysics, Gupta, H. (ed.), Springer.

is typically assumed to be destroyed quickly at high temperatures, or left preserved (frozen in) at low temperatures/small velocity gradients. The decrease in radial anisotropy toward the surface (Figure 2b) may therefore be associated with tectonically older, frozen in structure. On the scales accessible by surface wave studies, for example, anisotropy in old lithospheric domains may be less well aligned into the vertical, or into a coherent horizontal orientation than in the asthenosphere which is shaped by current mantle convection (*e.g. Fouch and Rondenay*, 2006).

At larger mantle depths, radial anisotropy becomes less well constrained (*e.g. Visser et al.*, 2008). There is some indication that radial anomalies pick up around the transition zone (Figure 1), and several studies have argued for the existence of azimuthal anisotropy around 660 km (*e.g. Trampert and van Heijst*, 2002; *Wookey et al.*, 2002). Most of the lower mantle is nearly isotropic until the D" region close to the core mantle boundary where there is good evidence for the existence of anisotropy from regional studies (*e.g. Moore et al.*, 2004), and indications for average radial anisotropy from global studies (*Boschi and Dziewoński*, 2000; *Panning and Romanowicz*, 2006). As for the upper mantle, one may invoke an LPO reactivation of dislocation creep, for example in cold, highly deformed subduction slabs (see Figure 1; *McNamara et al.*, 2002). The other, at present perhaps equally likely, mechanism that has been invoked for D" anisotropy is the alignment of melt tubules (SPO). Melt alignment may also play a role in the transition zone if the latter represents a melt-rich water filter (*Bercovici and Karato*, 2003). The D" region is expected to be at least as dynamically complex as the upper thermal boundary layer, and both domains are affected by compositional anomalies. Those include the continental lithosphere, with its stiff, compositionally anomalous and presumably neutrally buoyant cratonic keels, and likely piles of dense material at the base of the mantle in regions displaced along the CMB from recent subduction (*e.g. Garnero*, 2004; *Garnero and McNamara*, 2008). We therefore expect significant lateral variations in the generation of anisotropy within D" depending on the vertical flow setting (Figure 1, *e.g. Moore et al.*, 2004). Close to the CMB, anisotropy may also vary with depth depending on if lower mantle material has transitioned to the post-perovskite phase (*e.g. Wookey et al.*, 2005; *Merkel et al.*, 2007).

There is also robust evidence for anisotropy within the Earth's core. Body waves that traverse the inner core and are aligned with the rotation axis arrive earlier than those that cross in the equatorial plane (*Morelli et al.*, 1986). Evidence for anisotropy is also seen in the splitting of normal modes (*Woodhouse et al.*, 1986), and more recent data and models for core anisotropy are discussed in *Tromp* (2001) and *Souriau* (2007). However, there are still debates on the exact nature of the anisotropy distribution with depth (*cf. Ishii and Dziewoński*, 2003). Figure 1 shows radial, shear wave anisotropy for the inner core from *Beghein and Trampert* (2003). This particular model invoked a hexagonal close-packed phase of iron in the upper half of the inner core, and perhaps a transition into a different iron phase at depth, and predicts large amplitudes of radial anisotropy compared to the upper mantle. The origin of inner core anisotropy is also less clear than for the upper mantle (*Mainprice*, 2007). One hypothesis that has recently been discussed in some detail is freezing in of convective patterns during the cooling and evolution of the inner core (*Jeanloz and Wenk*, 1988; *Buffett*, 2009; *Deguen and Cardin*, 2009).

Becker, T. W. (2010): Seismic Anisotropy, In: Encyclopedia of Solid Earth Geophysics, Gupta, H. (ed.), Springer.

Structure and dynamics of the upper boundary layer

Seismic anisotropy at every depth range throughout the Earth holds valuable information on the dynamics of the planet. The connections can be made quantitative most easily for the shallower layers where seismological constraints abound, rock deformation is accessible via laboratory experiments, and geodynamic modeling is fairly well constrained. In the case of crack anisotropy in the shallow crust, observations yield constraints on regional stress fields. Applications include industry work (vertical seismic profiling in boreholes), earthquake studies around faults, and volcano monitoring where cracking due to magma migration can be traced.

Within the upper convective boundary layer, the oceanic plate domains (see *Lithosphere, oceanic*) should most closely resemble the simplified view of radial and azimuthal anisotropy due to LPO anisotropy formation in mantle flow as shown in Figure 1. *Gaboret et al.* (2003), *Becker et al.* (2003), and *Behn et al.* (2004) showed that mantle circulation from geodynamic models does indeed provide a valid explanation for azimuthal anisotropy patterns (Figure 2a), and that comparison of model predictions with anisotropy can yield constraints on mantle flow, such as the role of buoyant mantle upwellings as opposed to plate-induced shear. *Becker et al.* (2008) provided a quantitative model of radial anisotropy, and Figure 2b shows the fit of their preferred model to radial anisotropy averages in the upper mantle, as well as lateral patterns in azimuthal and radial anisotropy. Results are consistent with the expectation that the geodynamic models should describe recent (few 10s of Myr) asthenospheric flow best. The correlations between geodynamics and the seismological models (Figure 2b) is comparable or better than the match between different seismological models. Such first-order agreement between global geodynamics and seismology motivates current modeling efforts, for example on constraining the amount of net rotations of the lithosphere or the degree of lateral viscosity variations (*e.g. Becker*, 2008; *Conrad et al.*, 2007; *Conrad and Behn*, 2010; *Kreemer*, 2009).

Figure 2b shows that geodynamic models typically under-predict radial anisotropy in the shallower parts of the lithosphere, which is mainly due to continental domains. While anisotropy in younger continental lithosphere such as in the western United States appears to be well described by asthenospheric flow, older regions show more complex behavior such as a consistent orientation of seismic anisotropy over several hundred kilometers (*e.g. Babuška and Plomerová*, 2006). It has been suggested that anisotropy is concentrated in, and frozen into, the continental lithosphere, or, alternatively, that radial anisotropy is largest right underneath the mechanical boundary layer formed by stiff continents (*e.g. Gaherty and Jordan*, 1995; *Gung et al.*, 2003; *Fouch and Rondenay*, 2006). Figure 3 shows a profile through North America; anisotropy, as inferred from these models, only partially conforms to the simplified expectations (*cf. Panning and Romanowicz*, 2006). The cross section of radial anisotropy shows the expected focusing of SH faster than SV in the Pacific plate, and some regionally enhanced $v_{SH} > v_{SV}$ within the eastern United States and the Canadian craton, but no enhanced anisotropy beneath what would be inferred to be the base of the continental lithosphere from the isotropic anomalies. Azimuthal anisotropy is also, expectedly, strong within the Pacific plate (compare Figure 2a), but there is an intriguing low azimuthal anisotropy channel within the eastern North American continental lithosphere. If such features are due to complex tectonic deformation with small lateral shear-coherence, or due to the averaging properties of surface waves and incomplete ray illumination, remains to be determined. The study of continental anisotropy is

Becker, T. W. (2010): Seismic Anisotropy, In: Encyclopedia of Solid Earth Geophysics, Gupta, H. (ed.), Springer.

an active area of research, and many questions such as to the vertical coherence of lithospheric deformation and the depth extent of fault zone localization will benefit from the information that seismic anisotropy can bring to the table. There are numerous other, regional tectonic settings where anisotropy can yield important constraints, and those cannot be comprehensively reviewed here. Important examples include continental transforms and collision zones, spreading centers, and subduction zones. Reviews of our current understanding of such settings can be found in *Silver* (1996); *Savage* (1999); *Park and Levin* (2002) and *Long and Silver* (2009).

Powerful dynamic insights notwithstanding, there are still large uncertainties in every step of the chain of modeling that has to be followed. Complexities arise from inferring mantle flow from geodynamics (*e.g.* role of chemical *vrs.* thermal buoyancy, uncertainties about rheology), to predicting LPO textures (*e.g.* proper micro physical treatment), to inferring elasticity tensors (*e.g.* homogenization and temperature/pressure derivatives), to mapping those tensors in 3D to whatever seismological observable (preferred) or seismological model (more common) is used to benchmark the models (*e.g.* finite frequency wave propagation, sampling). The finding that overall patterns appear to be well explained (Figure 2), and that synthetic LPOs match those of xenolith samples provide some *a posterior* justification for the modeling rationale. Moreover, these agreements indicate that the bulk of the asthenospheric flow is indeed dominated by dry, A-type fabrics. However, future refinements of seismological imaging, for example through array deployments such as EarthScope USArray and temporary seafloor studies, theoretical developments in seismology, and the improved geodynamic treatment of anisotropy will undoubtedly lead to adjustment of our understanding of whole Earth anisotropic structure.

Summary

Seismic anisotropy is ubiquitous throughout the Earth and provides constraints on dynamic processes, from the stress in the crust, the origin and evolution of the continental lithosphere, through convective flow in the upper mantle, to core evolution. The state of upper-mantle geodynamic modeling is such that important questions, such as about absolute plate motion reference frames, intraplate deformation, or the hydration state of the mantle can be addressed. Important issues about the resolution of different seismological datasets and degree of robustness of seismological images remain. Joint with the inherent uncertainties in geodynamic modeling and how to map flow into seismic anisotropy, this means that numerous questions for the interpretation of anisotropy observable are open. This challenge mandates further theoretical and instrumentational efforts and that the study of anisotropy proceeds interdisciplinary and in a dynamics context. Answering those questions holds the promise of arriving at a new understanding of the workings of the mantle system.

Thorsten Becker

Acknowledgements

Detailed comments by Donna Blackman, Mark Behn, and Sergei Lebedev and valuable suggestions from Lapo Boschi, Sebastien Chevrot, David Okaya, Mark Panning, Vera Schulte-Pelkum, and an anonymous reviewer helped improve this contribution.

References

Abt, D. L., and K. M. Fischer (2008), Resolving three-dimensional anisotropic structure with shear-wave splitting tomography, *Geophys. J. Int.*, *173*, 859–886.

Anderson, D. L. (1966), Recent evidence concerning the structure and composition of the Earth's mantle, in *Physics and Chemistry of the Earth*, vol. 6, pp. 1–131, Pergmanon Press, Oxford UK.

Anderson, D. L. (1989), *Theory of the Earth*, Blackwell Scientific Publications, Boston, available online at `http://caltechbook.library.caltech.edu/14/1/TheoryoftheEarth.pdf`, accessed 01/2010.

Ando, M., Y. Ishikawa, and F. Yamasaki (1983), Shear-wave polarization anisotropy in the mantle beneath Honshu, Japan, *J. Geophys. Res.*, *88*, 5850–5864.

Babuška, V., and M. Cara (1991), *Seismic Anisotropy in the Earth*, Kluwer Academic Publishers, Dordrecht.

Babuška, V., and J. Plomerová (2006), European mantle lithosphere assembled from rigid microplates with inherited seismic anisotropy, *Phys. Earth Planet. Inter.*, *158*, 264–280.

Babuška, V., J. Plomerová, and J. Šíleny (1984), Spatial variations of P residuals and deep structure of the European lithospere, *Geophys. J. R. Astr. Soc.*, *79*, 363–383.

Backus, G. E. (1965), Possible forms of seismic anisotropy of the uppermost mantle under oceans, *J. Geophys. Res.*, *70*, 3429–3439.

Becker, T. W. (2008), Azimuthal seismic anisotropy constrains net rotation of the lithosphere, *Geophys. Res. Lett.*, *35*, doi:10.1029/2007GL032928, correction: doi:10.1029/2008GL033946.

Becker, T. W., J. B. Kellogg, G. Ekström, and R. J. O'Connell (2003), Comparison of azimuthal seismic anisotropy from surface waves and finite-strain from global mantle-circulation models, *Geophys. J. Int.*, *155*, 696–714.

Becker, T. W., S. Chevrot, V. Schulte-Pelkum, and D. K. Blackman (2006), Statistical properties of seismic anisotropy predicted by upper mantle geodynamic models, *J. Geophys. Res.*, *111*(B08309), doi:10.1029/2005JB004095.

Becker, T. W., B. Kustowski, and G. Ekström (2008), Radial seismic anisotropy as a constraint for upper mantle rheology, *Earth Planet. Sci. Lett.*, *267*, 213–237.

Beghein, C., and J. Trampert (2003), Robust normal mode constraints on inner-core anisotropy from model space search, *Science*, *299*, 552–555.

Behn, M. D., C. P. Conrad, and P. G. Silver (2004), Detection of upper mantle flow associated with the African Superplume, *Earth Planet. Sci. Lett.*, *224*, 259–274.

Bercovici, D., and S.-i. Karato (2003), Whole-mantle convection and the transition-zone water filter, *Nature*, *425*, 39–44.

Blackman, D. (2007), Use of mineral physics, with geodynamic modelling and seismology, to investigate flow in the Earth's mantle, *Rep. Prog. Phys.*, *70*, 659–689.

Bokelmann, G. H. R. (2002), Convection-driven motion of the north American craton: evidence from P-wave anisotropy, *Geophys. J. Int.*, *148*, 278–287.

Boschi, L., and A. M. Dziewoński (2000), Whole Earth tomography from delay times of P, PcP, PKP phases: lateral heterogeneities in the outer core, or radial anisotropy in the mantle?, *J. Geophys. Res.*, *105*, 25,567–25,594.

Browaeys, J., and S. Chevrot (2004), Decomposition of the elastic tensor and geophysical applica-

Becker, T. W. (2010): Seismic Anisotropy, In: Encyclopedia of Solid Earth Geophysics, Gupta, H. (ed.), Springer.

tions, *Geophys. J. Int.*, *159*, 667–678.

Buffett, B. (2009), Onset and orientation of convection in the inner core, *Geophys. J. Int.*, *179*, 711–719.

Chastel, Y. B., P. R. Dawson, H.-R. Wenk, and K. Bennett (1993), Anisotropic convection with implications for the upper mantle, *J. Geophys. Res.*, *98*, 17,757–17,771.

Chevrot, S. (2006), Finite-frequency vectorial tomography: a new method for high-resolution imaging of upper mantle anisotropy, *Geophys. J. Int.*, *165*, 641–657.

Chevrot, S., and V. Monteiller (2009), Principles of vectorial tomography – the effects of model parametrization and regularization in tomographic imaging of seismic anisotropy, *Geophys. J. Int.*, *179*, 1726–1736.

Christensen, N. I., and W. D. Mooney (1995), Seismic velocity structure and composition of the continental crust: A global review, *J. Geophys. Res.*, *100*, 9761–9788.

Christensen, U. R. (1987), Some geodynamical effects of anisotropic viscosity, *Geophys. J. R. Astr. Soc.*, *91*, 711–736.

Conrad, C. P., and M. Behn (2010), Constraints on lithosphere net rotation and asthenospheric viscosity from global mantle flow models and seismic anisotropy, *Geochemistry, Geophysics, Geosystems*, *11*(Q05W05), doi:10.1029/2009GC002970.

Conrad, C. P., M. D. Behn, and P. G. Silver (2007), Global mantle flow and the development of seismic anisotropy: differences between the oceanic and continental upper mantle, *J. Geophys. Res.*, *112*, doi:10.1029/2006JB004608.

Crampin, S., and S. Chastin (2003), A review of shear wave splitting in the crack-critical crust, *Geophys. J. Int.*, *155*, 221–240.

Deguen, R., and P. Cardin (2009), Tectonic history of the Earth's inner core preserved in its seismic structure, *Nature Geosc.*, *2*, 419–422.

Deschamps, F., S. Lebedev, T. Meier, and J. Trampert (2008), Azimuthal anisotropy of Rayleigh-wave phase velocities in the east-central United States, *Geophys. J. Int.*, *173*, 827–843.

Dziewoński, A. M., and D. L. Anderson (1981), Preliminary reference Earth model, *Phys. Earth Planet. Inter.*, *25*, 297–356.

Ekström, G., and A. M. Dziewonski (1998), The unique anisotropy of the Pacific upper mantle, *Nature*, *394*, 168–172.

Forsyth, D. W. (1975), The early structural evolution and anisotropy of the oceanic upper mantle, *Geophys. J. R. Astr. Soc.*, *43*, 103–162.

Fouch, M. (2006), Upper mantle anisotropy database, Online, accessed in 06/2006, `http://geophysics.asu.edu/anisotropy/upper/`.

Fouch, M. J., and S. Rondenay (2006), Seismic anisotropy beneath stable continental interiors, *Phys. Earth Planet. Inter.*, *158*, 292–320.

Gaboret, C., A. M. Forte, and J.-P. Montagner (2003), The unique dynamics of the Pacific Hemisphere mantle and its signature on seismic anisotropy, *Earth Planet. Sci. Lett.*, *208*, 219–233.

Gaherty, J. B., and T. H. Jordan (1995), Lehmann discontinuity as the base of an anisotropic layer beneath continents, *Science*, *268*, 1468–1471.

Gaherty, J. B., T. H. Jordan, and L. S. Gee (1996), Seismic structure of the upper mantle in a central Pacific corridor, *J. Geophys. Res.*, *101*, 22,291–22,310.

Becker, T. W. (2010): Seismic Anisotropy, In: Encyclopedia of Solid Earth Geophysics, Gupta, H. (ed.), Springer.

Garnero, E. J. (2004), A new paradigm for Earth's core-mantle boundary, *Science*, *304*, 835–836.

Garnero, E. J., and A. K. McNamara (2008), Structure and dynamics of the Earth's lower mantle, *Science*, *320*, 626–628.

Gung, Y., M. Panning, and B. Romanowicz (2003), Global anisotropy and the thickness of continents, *Nature*, *422*, 707–711.

Hager, B. H., and R. J. O'Connell (1981), A simple global model of plate dynamics and mantle convection, *J. Geophys. Res.*, *86*, 4843–4867.

Hearmon, R. F. S. (1961), *An introduction to applied anisotropic elasticity*, Oxford University Press, London.

Hess, H. H. (1964), Seismic anisotropy of the uppermost mantle under oceans, *Nature*, *203*, 629–631.

Holtzman, B. K., D. L. Kohlstedt, M. E. Zimmerman, F. Heidelbach, T. Hiraga, and J. Hustoft (2003), Melt segregation and strain partitioning: Implications for seismic anisotropy and mantle flow, *Science*, *301*, 1227–1230.

Ishii, M., and A. M. Dziewoński (2003), Distinct seismic anisotropy at the centre of the earth, *Phys. Earth Planet. Inter.*, *140*, 203–217.

Jeanloz, R., and H. R. Wenk (1988), Convection and anisotropy of the inner core, *Geophys. Res. Lett.*, *15*, 72–75.

Kaminski, É., and N. M. Ribe (2001), A kinematic model for for recrystallization and texture development in olivine polycrystals, *Earth Planet. Sci. Lett.*, *189*, 253–267.

Karato, S.-i. (1992), On the Lehmann discontinuity, *Geophys. Res. Lett.*, *51*, 2255–2258.

Karato, S.-i., H. Jung, I. Katayama, and P. Skemer (2008), Geodynamic signficance of seismic anisotropy of the upper mantle: new insights from laboratory studies, *Ann Rev. Earth Planet. Sci.*, *36*, 59–95.

Kreemer, C. (2009), Absolute plate motions constrained by shear wave splitting orientations with implications for hot spot motions and mantle flow, *J. Geophys. Res.*, *114*(B10405), doi:10.1029/2009JB006416.

Kustowski, B., G. Ekström, and A. M. Dziewoński (2008), Anisotropic shear-wave velocity structure of the Earth's mantle: A global model, *J. Geophys. Res.*, *113*, doi:10.1029/2007JB005169.

Lebedev, S., and R. D. van der Hilst (2008), Global upper-mantle tomography with the automated multimode inversion of surface and S-wave forms, *Geophys. J. Int.*, *173*, 505–518.

Lev, E., and B. H. Hager (2008), RayleighTaylor instabilities with anisotropic lithospheric viscosity, *Geophys. J. Int.*, *173*, 806–814.

Levin, V., and J. Park (1998), $P-SH$ conversions in layered media with hexagonally symmetric anisotropy: A cookbook, *Pure Appl. Geophys.*, *151*, 669–697.

Lin, F., M. P. Moschetti, and M. H. Ritzwoller (2008), Surface wave tomography of the western United States from ambient seismic noise: Rayleigh and Love wave phase velocity maps, *Geophys. J. Int.*, *173*, 281–298.

Long, M. D., and T. W. Becker (2010), Mantle dynamics and seismic anisotropy, *Earth Planet. Sci. Lett.*, *submitted*, available online at `http://geodynamics.usc.edu/~becker/preprints/lb10.pdf`.

Long, M. D., and P. G. Silver (2009), Shear wave splitting and mantle anisotropy: Measurements, interpretations, and new directions, *Surv. Geophys.*, *30*, 407–461.

Long, M. D., M. V. de Hoop, and R. D. van der Hilst (2008), Wave equation shear wave splitting tomography, *Geophys. J. Int.*, *172*, 311–330.

Love, A. E. H. (1927), *A Treatise on the Mathematical Theory of Elasticity*, Cambridge University Press, Cambridge, reprinted in 1944 by Dover Publications, New York.

Mainprice, D. (2007), Seismic anisotropy of the deep Earth from a mineral and rock physics perspective, in *Treatise on Geophysics*, vol. 2, edited by G. Schubert and D. Bercovici, pp. 437–492, Elsevier.

Mainprice, D., and A. Nicholas (1989), Development of shape and lattice preferred orientations: application to the seismic anisotropy of the lower crust, *J. Struct. Geol.*, *11*, 175–189.

Marone, F., and F. Romanowicz (2007), The depth distribution of azimuthal anisotropy in the continental upper mantle, *Nature*, *447*, 198–201.

McKenzie, D. P. (1979), Finite deformation during fluid flow, *Geophys. J. R. Astr. Soc.*, *58*, 689–715.

McNamara, A. K., P. E. van Keken, and S.-i. Karato (2002), Development of anisotropic structure in the Earth's lower mantle by solid-state convection, *Nature*, *416*, 310–314.

Meissner, R., W. D. Mooney, and I. Artemieva (2002), Seismic anisotropy and mantle creep in young orogens, *Geophys. J. Int.*, *149*, 1–14.

Meissner, R., W. Rabbel, and H. Kern (2006), Seismic lamination and anisotropy of the lower continental crust, *Tectonophysics*, *416*, 81–99.

Merkel, S., A. K. McNamara, A. Kubo, S. Speziale, L. Miyagi, Y. Meng, T. S. Duffy, and H.-R. Wenk (2007), Deformation of (Mg,Fe)SiO_3 post-perovskite and D" anisotropy, *Science*, *316*(5832), 1729–32.

Montagner, J.-P. (2007), Upper mantle structure: Global isotropic and anisotropic elastic tomography, in *Treatise on Geophysics*, vol. 1, edited by G. Schubert and D. Bercovici, pp. 559–589, Elsevier.

Montagner, J. P., and D. L. Anderson (1989), Petrological constraints on seismic anisotropy, *Phys. Earth Planet. Inter.*, *54*, 82–105.

Montagner, J.-P., and H.-C. Nataf (1986), A simple method for inverting the azimuthal anisotropy of surface waves, *J. Geophys. Res.*, *91*, 511–520.

Montagner, J. P., and H. C. Nataf (1988), Vectorial tomography-I. Theory, *Geophys. J.*, *94*, 295–307.

Montagner, J.-P., D.-A. Griot-Pommera, and J. Laveé (2000), How to relate body wave and surface wave anisotropy?, *J. Geophys. Res.*, *105*, 19,015–19,027.

Moore, M. M., E. J. Garnero, T. Lay, and Q. Williams (2004), Shear wave splitting and waveform complexity for lowermost mantle structures with low-velocity lamellae and transverse isotropy, *J. Geophys. Res.*, *103*, doi:10.1029/2003JB002546.

Morelli, A., A. M. Dziewonski, and J. H. Woodhouse (1986), Anisotropy of the inner core inferred from PKIKP travel times, *Geophys. Res. Lett.*, *13*, 1545–1548.

Nataf, H.-C., I. Nakanishi, and D. L. Anderson (1984), Anisotropy and shear velocity heterogeneity in the upper mantle, *Geophys. Res. Lett.*, *11*, 109–112.

Nye, J. F. (1985), *Physical Properties of Crystals*, Oxford University Press, London.

Panning, M., and B. Romanowicz (2006), A three-dimensional radially anisotropic model of shear velocity in the whole mantle, *Geophys. J. Int.*, *167*, 361–379.

Becker, T. W. (2010): Seismic Anisotropy, In: Encyclopedia of Solid Earth Geophysics, Gupta, H. (ed.), Springer.

Panning, M. P., and G. Nolet (2008), Surface wave tomography for azimuthal anisotropy in a strongly reduced parameter space, *Geophys. J. Int.*, *174*, 629–648.

Park, J., and V. Levin (2002), Seismic anisotropy: Tracing plate dynamics in the mantle, *Science*, *296*, 485–489.

Podolefsky, N. S., S. Zhong, and A. K. McNamara (2004), The anisotropic and rheological structure of the oceanic upper mantle from a simple model of plate shear, *Geophys. J. Int.*, *158*, 287–296.

Saltzer, R. L., J. B. Gaherty, and T. H. Jordan (2000), How are vertical shear wave splitting measurements affected by variations in the orientation of azimuthal anisotropy with depth?, *Geophys. J. Int.*, *141*, 374–390.

Savage, M. (1998), Lower crustal anisotropy or dipping boundaries? Effects on receiver functions and a case study in New Zealand, *J. Geophys. Res.*, *103*, 15,069–15,087.

Savage, M. K. (1999), Seismic anisotropy and mantle deformation: What have we learned from shear wave splitting?, *Rev. Geophys.*, *37*, 65–106.

Schulte-Pelkum, V., and D. K. Blackman (2003), A synthesis of seismic P and S anisotropy, *Geophys. J. Int.*, *154*, 166–178.

Schulte-Pelkum, V., G. Masters, and P. M. Shearer (2001), Upper mantle anistropy from long-period P polarization, *J. Geophys. Res.*, *106*, 21,917–21,934.

Sieminski, A., J. Trampert, and J. Tromp (2009), Principal component analysis of anisotropic finite-frequency sensitivity kernels, *Geophys. J. Int.*, *179*, 1186–1198.

Šíleny, J., and J. Plomerová (1996), Inversion of shear-wave splitting parameters to retrieve three-dimensional orientation of anisotropy in continental lithosphere, *Phys. Earth Planet. Inter.*, *95*, 277–292.

Silver, P. G. (1996), Seismic anisotropy beneath the continents: probing the depths of geology, *Ann. Rev. Earth Planet. Sci.*, *24*, 385–432.

Silver, P. G., and Chan (1991), Shear wave splitting and subcontinental mantle deformation, *J. Geophys. Res.*, *96*, 16,429–16,454.

Smith, D. B., M. H. Ritzwoller, and N. M. Shapiro (2004), Stratification of anisotropy in the Pacific upper mantle, *J. Geophys. Res.*, *109*, doi:10.1029/2004JB003200.

Smith, G. P., and G. Ekström (1999), A global study of P_n anisotropy beneath continents, *J. Geophys. Res.*, *104*, 963–980.

Smith, M. L., and F. A. Dahlen (1973), The azimuthal dependence of Love and Rayleigh wave propagation in a slightly anisotropic medium, *J. Geophys. Res.*, *78*, 3321–3333.

Souriau, A. (2007), The Earth's core, in *Treatise on Geophysics*, vol. 1, edited by B. Romanowicz and A. Dziewonski, pp. 655–693, Elsevier, Amsterdam.

Tanimoto, T., and D. L. Anderson (1984), Mapping convection in the mantle, *Geophys. Res. Lett.*, *11*, 287–290.

Tanimoto, T., and D. L. Anderson (1985), Lateral heterogeneity and azimuthal anisotropy of the upper mantle: Love and Rayleigh waves 100–250 s, *J. Geophys. Res.*, *90*, 1842–1858.

Thomsen, L. (1986), Weak elastic anisotropy, *Geophysics*, *51*, 1954–1966.

Tommasi, A., M. Knoll, A. Vauchez, J. Sgnorelli, C. Thoraval, and R. Ioge (2009), Structural reactivation in plate tectonics controlled by olivine crystals anisotropy, *Nature Geosc.*, *2*, 423–427.

Trampert, J., and H. J. van Heijst (2002), Global azimuthal anisotropy in the transition zone, *Science*,

Becker, T. W. (2010): Seismic Anisotropy, In: Encyclopedia of Solid Earth Geophysics, Gupta, H. (ed.), Springer.

296, 1297–1299.

Tromp, J. (2001), Inner core anisotropy and rotation, *Annu. Rev. Earth Planet. Sci.*, *29*, 47–69.

Vinnik, L., G. L. Kosarev, and L. I. Makeyeva (1984), Anisotropy of the lithosphere from the observations of SKS and $SKKS$ phases, *Proc. Acad. Sci. USSR*, *278*, 1335–1339.

Visser, K., J. Trampert, S. Lebedev, and B. L. N. Kennett (2008), Probability of radial anisotropy in the deep mantle, *Earth Planet. Sci. Lett.*, *270*, 241–250.

Weiss, T., S. Siegesmund, W. Rabbel, T. Bohlen, and M. Pohl (1999), Seismic velocities and anisotropy of the lower continental crust: A review, *Pure Appl. Geophys.*, *156*, 97–122.

Woodhouse, J. H., D. Giardini, and X.-D. Li (1986), Evidence for inner core anisotropy from free oscillations, *Geophys. Res. Lett.*, *13*, 1549–1552.

Wookey, J., J.-M. Kendall, and G. Barruol (2002), Mid-mantle deformation inferred from seismic anisotropy, *Nature*, *415*, 777–780.

Wookey, J., S. Stackhouse, J.-M. Kendall, J. Brodholt, and G. D. Price (2005), Efficacy of the post-perovskite phase as an explanation for lowermost-mantle seismic properties, *Nature*, *438*, 1004–1007.

Wüstefeld, A., G. H. R. Bokelmann, G. Barruol, and J. P. Montagner (2009), Identifying global seismic anisotropy patterns by correlating shear-wave splitting and surface-wave data, *Phys. Earth Planet. Inter.*, *176*, 198–212.

Cross-references

- Body waves
- Correlation techniques, ambient noise
- Earthquake tomography
- Elasticity and wave propagation
- Free oscillations of the Earth
- Inverse theory
- Lithosphere, oceanic
- Lithosphere, continental
- Mantle convection
- Mantle D” Layer
- Mantle rheology
- Seismic, receiver function technique
- Seismic structure of the Earth, global models
- Shear wave splitting
- Surface waves

Becker, T. W. (2010): Seismic Anisotropy, In: Encyclopedia of Solid Earth Geophysics, Gupta, H. (ed.), Springer.

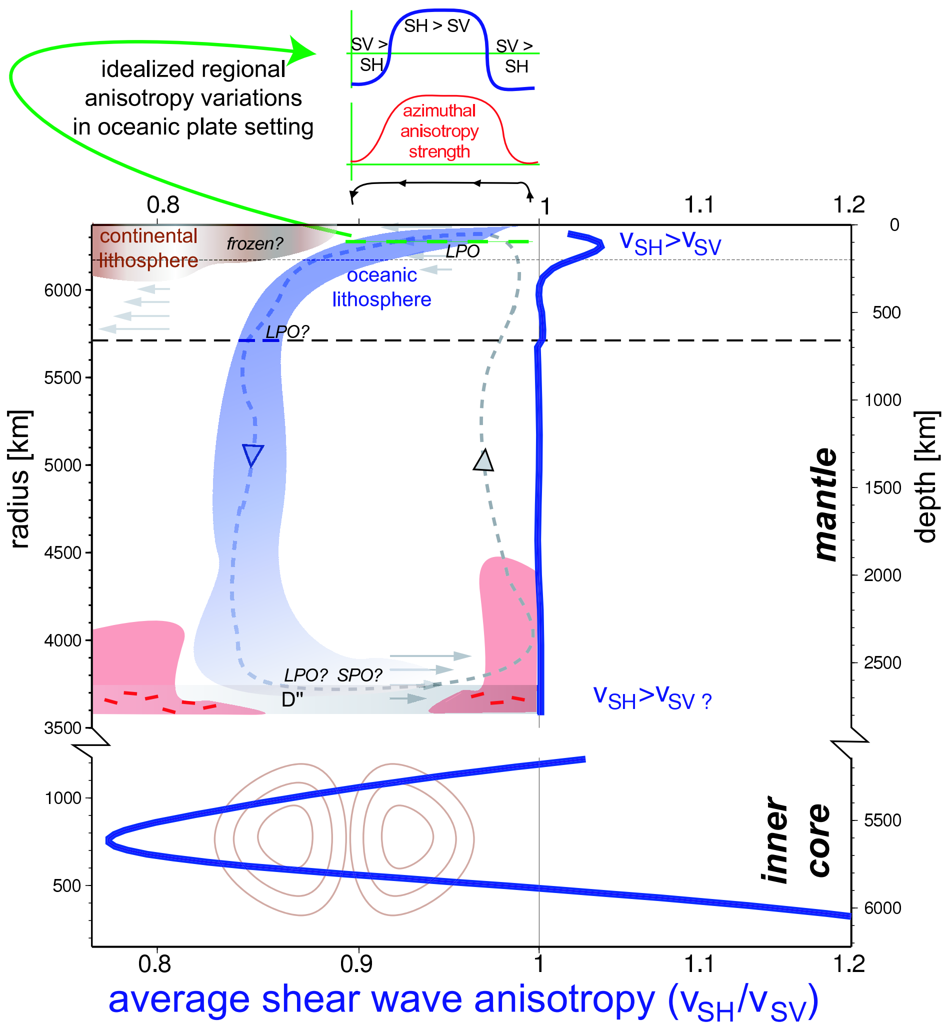

Figure 1: Cartoon of the possible distribution of whole Earth anisotropy (note scale break at CMB) with geodynamic interpretation (*cf. Montagner*, 2007); dotted and dashed horizontal lines indicate 200 and 660 km depths, respectively. The heavy blue lines in center show average radial anisotropy from *Kustowski et al.* (2008) for the mantle and from *Beghein and Trampert* (2003) for the inner core. Underneath oceanic plates, mantle flow is primarily horizontal, leading to LPO anisotropy alignment with $v_{SH} > v_{SV}$, while the radial mass transport associated with upwellings and downwellings may lead locally $v_{SV} > v_{SH}$. Beneath continental regions, both frozen-in anisotropy from past tectonic deformation and asthenospheric anisotropy from present-day convection may contribute. The gray, dashed, circular line in the mantle indicates an idealized flow trajectory for a downwelling slab (blue) displacing a thermo-chemical "pile" (red) at the core mantle boundary (*cf. Garnero and McNamara*, 2008). This deep flow may affect CMB dynamics and lead to LPO and/or SPO anisotropy (modified from *Long and Becker*, 2010).

Becker, T. W. (2010): Seismic Anisotropy, In: Encyclopedia of Solid Earth Geophysics, Gupta, H. (ed.), Springer.

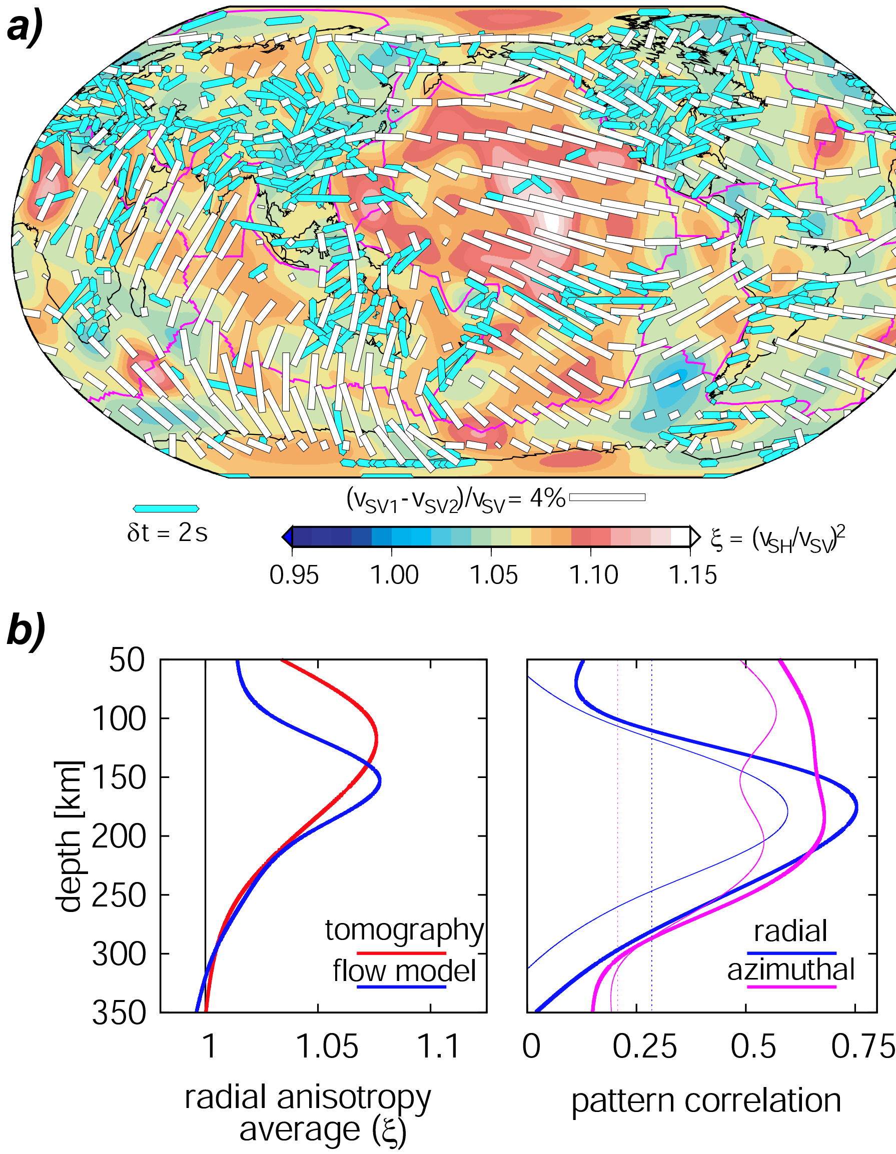

Figure 2: Global, uppermost mantle seismic anisotropy. a) Seismological constraints: Radial (background, from *Kustowski et al.*, 2008) and azimuthal anisotropy (white sticks indicating fast orientation, from *Lebedev and van der Hilst*, 2008) at 150 km, as well as *SKS* splitting (cyan sticks). *SKS* data are shown as a simple 5° average of the compilations by *Fouch* (2006) and *Wüstefeld et al.* (2009), but note that such averaging only provides a simplified view of azimuthal anisotropy (see text, and *Schulte-Pelkum and Blackman*, 2003, for example). b) Radial anisotropy layer averages, on left, for the seismological model of *Kustowski et al.* (2008) and as predicted from the best-fitting geodynamic model of *Becker et al.* (2008). On right, pattern correlations up to spherical harmonic degree 8 between the same geodynamic model and radial (from *Kustowski et al.*, 2008) and azimuthal (from *Lebedev and van der Hilst*, 2008) seismic tomography. Heavy and thin lines denote oceanic-lithosphere only and global correlations, respectively. Vertical, dashed lines show 95% significance level (modified from *Long and Becker*, 2010).

Becker, T. W. (2010): Seismic Anisotropy, In: Encyclopedia of Solid Earth Geophysics, Gupta, H. (ed.), Springer.

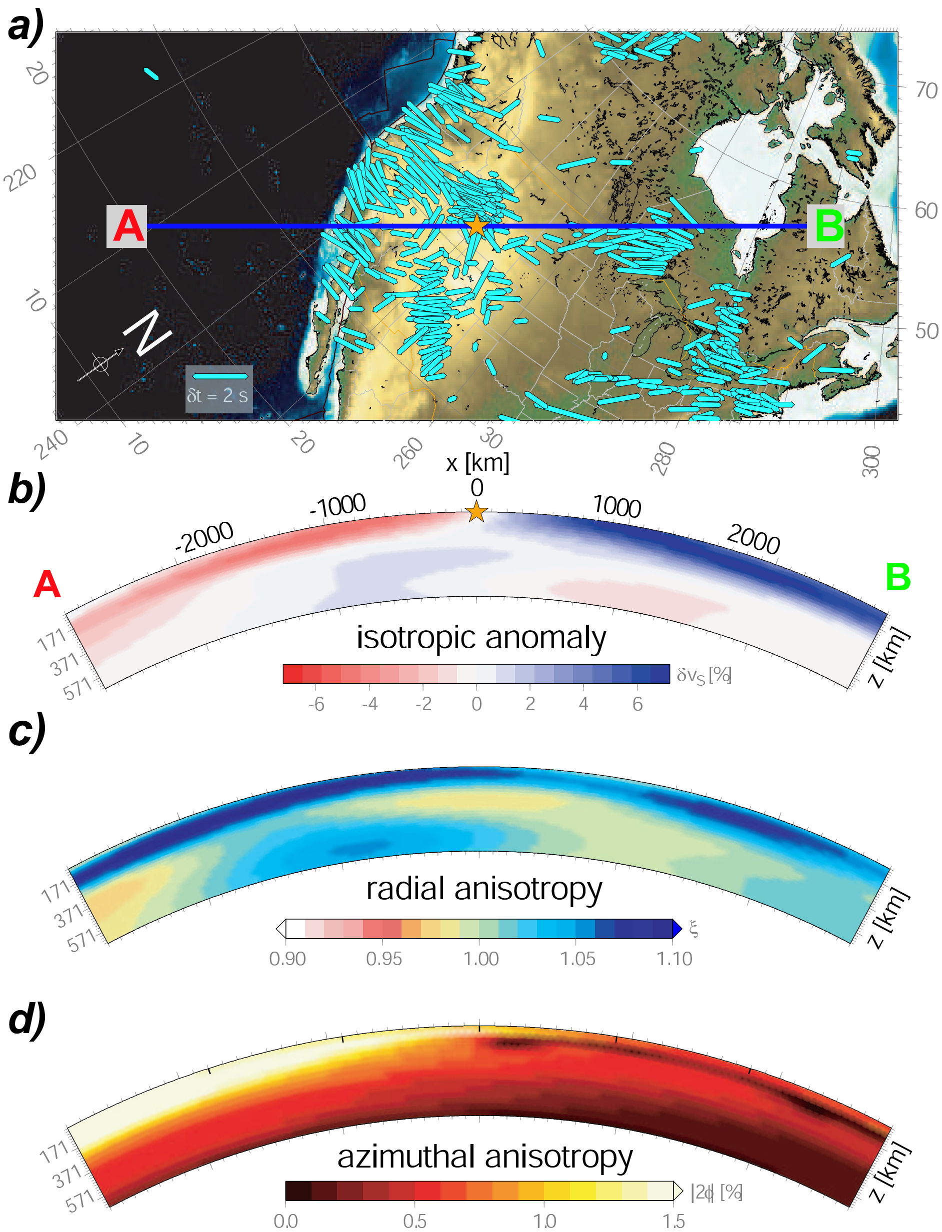

Figure 3: Pacific and North American upper mantle anisotropy. a) *SKS* splitting (as in Figure 2, but averaged by 0.5°) and location of cross-continental profile; b) isotropic shear wave velocity relative to background (Voigt average, from *Kustowski et al.*, 2008); c) radial anisotropy ($\xi = (v_{SH}/v_{SV})^2$, from *Kustowski et al.*, 2008); and d) strength of azimuthal anisotropy ($|(v_{SV1} - v_{SV2})/v_{SV}|$, from *Lebedev and van der Hilst*, 2008). Figure is modified from *Long and Becker* (2010).